

www.chemistryselect.org

Microwave-Assisted Synthesis and Characterization of Some Aldehyde Derivatives of Imidazo[2,1-b][1,3,4]thiadiazole: Crystal Structure Insights, In-Silico and Biological Studies

Kunigal S. Sagar,^[a] Karthik Kumara,^[b] Banu SH,^[c] Neratur K. Lokanath,^[d] Manikyanahalli N. Kumara,^{*[a]} and Kempegowda Mantelingu^{*[e]}

The microwave-assisted synthesis, crystallographic studies, *insilico* docking and the evaluation of in-vitro biological activities of 2-(3,4-dimethoxy)-6-(substituted phenyl)- imidazo[2,1-b][1,3,4]thiadiazole-5-carbaldehydes is represented here. Single-crystal X-ray diffraction experiments were used to identify the crystal structure of the 6-(4-chlorophenyl)-2-(3,4-dimethoxybenzyl)imidazo[2,1-b][1,3,4]thiadiazole-5-carbaldehyde. Using fingerprint plots, Hirshfeld surface analysis was used to confirm the contributions of distinct intermolecular interactions in the development of the crystal packing. Further, density functional theory calculations were employed to calculate the molecule's electronic properties. The chemically active regions on the molecule are identified by analysing the molecular

electrostatic potential map. *in-silico* studies revealed that the molecules can be effectively used as antibacterial agents by taking the 3q82 receptor with chloramphenicol as a standard. As compared to the chloramphenicol standard, in-vitro tests showed that molecules **4a**, **4b**, **4c**, and **4f** had a zone of inhibition that ranged from 9 to 11 mm against both Grampositive (*Bacillus subtilis*) and Gram-negative (*Escherichia coli*) bacteria. The minimum inhibitory concentration was between 40 to 70 μ g/ml. These compounds' Hydroxyl free radical scavenging activity was between 40 to 85%. Whereas, DPPH radical scavenging activity was between 40 and 70%. Percentage hemolysis or cell protective activity of the compounds was ineffective at 20–40%.

Introduction

Microwave heating for chemical modification dates back to the 1950s, but it wasn't until identifications by the Gedye and Giguere/Majetich groups in 1986 that the technology gained general acceptance.^[1] In theory, the organic reactions have

[a] K. S. Sagar, Prof. M. N. Kumara
Chemistry Department
Yuvaraja's College (Constituent and Autonomous)
University of Mysore, Mysuru – 570005, India
E-mail: kumaramanikya73@gmail.com

- [b] Dr. K. Kumara Department of Physics B.M.S. College of Engineering Bengaluru – 560 019, India
- [c] Dr. B. SH

 Department of Biochemistry

 JSS College

 Mysuru. India
- [d] Prof. N. K. Lokanath Department of Studies in Physics Manasagangotri University of Mysore, Mysuru – 570006, India
- [e] Prof. K. Mantelingu
 Prof. K. Mantelingu
 Department of Studies in Chemistry
 Manasagangotri
 University of Mysore, Mysuru 570006, India
 E-mail: kmantelingu@chemistry.uni-mysore.ac.in
- Supporting information for this article is available on the WWW under https://doi.org/10.1002/slct.202302877

been rewritten with the use of microwaves as a non-conventional energy source. [2] Microwave synthesis [3] is considered an important approach towards green chemistry^[4] because this technique is more eco-friendly. Microwave irradiation has been used to improve different organic syntheses because it may couple directly with the reaction molecule and pass thermal conductivity, resulting in a rapid and even temperature rise. Microwave synthesis is a significant advancement in synthetic chemistry^[5] An important shift in the way chemical synthesis is accomplished. [6] Traditional heating has long been recognised as inefficient, time-consuming, and artistically limiting.[7] Here, we provide the results of a further investigation of this process, paying close attention to any variations between microwave and traditional heating. In contrast to conventional heating, MW irradiation conditions allow for the acceleration of organic reactions and the production of selective products.[8] Hightemperature homogeneity, instantaneous and rapid heating (deep interior heating), and selective heating are some of the benefits. [9] Chemical transformations aided by microwave irradiation frequently provide high yields along with straightforward handling and processing.[10]

Fused heterocyclic systems containing S and N as heteroatoms^[11] have increased in importance in the field of medicinal chemistry due to their broad spectrum of biological activities. The imidazo[2,1-b][1,3,4]thiadiazole bicycle system has imidazole and 1,3,4-thiadiazole moieties.^[12] Many imidazoles have been used since more than 70 years ago as Carbonic anhydrase inhibitor(CAI). Based on imidazo[2,1-b][1,3,4]thiadiazole ring^[13] medications have been used in

therapeutics, including acetazolamide, methazolamide, ethoxzolamide, and dorzolamide.[14] A powerful carbonic anhydrase inhibitor, methazolamide (Figure 1) (brand name Neptazane), is recommended for the treatment of elevated intraocular pressure (IOP) in chronic open-angle glaucoma and secondary glaucoma. The anti-tumour potential of the 2-amino-1,3,4thiadiazole skeleton is known for long and further its fused derivatives with imidazo[2,1-b] ring system has resulted in compounds exhibiting potential diuretics, [15] antiglaucoma, [16] anticonvulsant or antiinfective^[17] drug. Consequently, many imidazo[2,1-b][1,3,4]thiadiazole derivatives have been reported to possess antitumor properties and are known to exhibit a broad spectrum of biological activities such as antitubercular, [18] anaesthetic,[19] antibacterial,^{20]} anticonvulsant,^[21] inflammatory, [22] antifungal, [23] antipyretic, [24] anthelmintic, [25] analgesic, [26] cardiotonic, [27] leishmanicidal, [28] diuretic, [29] and herbicidal^[30] activities. Megazol (Figure 1) are veteran anthelmintic. Levamisole is an immune-modulator medication that selectively inhibits enzymes and is used to treat a variety of cancers, [31] expanding the use of these agents in contemporary drug design.[32] imidazothiadiazole derivatives have recently been reported to treat platelet aggregation (Figure 1). We envisioned synthesising a series of Imidazothiadiazole moieties and evaluating them for biological research in light of these discoveries and our ongoing interest[33-35] in the creation of various classes of heterocyclic bases.

The compound's crystal structure, which was established via single-crystal X-ray crystallography, [36,37] also supports this microwave method of synthesis. Hirshfeld surface analysis is used to quantify intermolecular interactions [38,39] using finger-print plots. The surface properties were analysed using 3D dnorm surfaces. [40] This research discusses the HOMO-LUMO energy gap, as well as crystal structure aspects such as 3D energy framework calculations and molecular lattice energy estimates, [41] and density functional theory (DFT) calculations. [42] Finally, the chemically active areas of the molecule are determined by studying the molecular electrostatic potential map.

We chose *in-silico* studies^[43] using the antibacterial *E. coli* receptor 3q82 against synthetic compounds with chloramphenicol as standard in order to understand the binding interactions of synthesized compounds on antibacterial activity. The more negative value exhibited by the compound (4f) was proved to be more potent than the standard which was confirmed experimentally. The *in-vitro* anti-oxidant activity was assessed using the hydroxyl radical scavenging activity and the

Figure 1. Drugs containing imidazothiadiazole as a key moiety.

DPPH radical scavenging activity^[44] of the synthesized compounds. Additionally, the hemolytic assay^[45] which measures the amount of hemoglobin released into the plasma as a sign of red blood cell lysis was carried out.

Procedure

Materials and methods

The solvents, chemicals, and reagents used were all from Sigma Aldrich, SD-Fine, Spectrochem, and Avra. Analytical methods such as 1H and 13C NMR, HRMS, and FT-IR were used to characterise the synthesised compounds. Using DMSO/CDCI3, Agilent 400 M Hz/Bruker 400 and 500 MHz spectrometers were used to capture 1H and 13C NMR spectra. Values for chemical shift (δ) are given in ppm. Regarding TMS, CDCl3 was employed as a solvent. Values for coupling constants (J) are given in Hz. Melting points were examined and found to be accurate. By using electrospray (ESI), mass spectra were obtained. TLC (commercially available pre-coated plates, MERCK 60 F254, 0.25 mm thickness) was used to monitor reactions while UV light was employed for visualisation. Column chromatography was performed on silica gel 60 (60-120 mesh). For column chromatography and TLC, the mobile phases utilized were hexane and ethyl acetate. The microwave experiments were conducted with Anton-Paar Monowave 200 equipment.

X-ray diffraction

For X-ray diffraction experiments, defect-free single crystal with acceptable dimensions of 0.29×0.24×0.22 mm³ were selected. A Rigaku XtaLAB Mini diffractometer with an X-ray generator running at 50 kV, 12 mA, and MoK radiation was used to gauge the crystals' X-ray intensity. Data were obtained with χ fixed at 54° and for various values of φ (0° and 360°), maintaining the scan width of 0.5° with an exposure period of 4 seconds, and the sample to detector distance was preserved at 50 mm. Crystal clear was used to assess the entire datasets of intensity data^[46] Utilising the SHELXS and SHELXL programmes, the crystal structure was solved using the direct technique and improved using the full-matrix least squares method on F2.[47] All the non-hydrogen atoms were refined anisotropically and the hydrogen atoms were positioned geometrically, with C-H= 0.91–1.04 Å and refined using a riding model with $U_{iso}(H) = 1.2$ $U_{\rm eq}(C)$, $U_{\rm iso}(H) = 1.5~U_{\rm eq}(C_{\rm methyl})$. The final difference is the result of multiple cycles of refinement. The residual is saturated to 0.0486 on the Fourier map, which displayed peaks without any chemical significance. The programme PLATON was used to perform the geometrical computations.[48] Using the software MERCURY, molecular and packing diagrams were created. [49]



In-silico molecular docking studies and biological activities

In-silico molecular docking^[50] was performed in accordance with previously described protocols. From the RCSB Protein Data Bank https://doi.org/10.2210/pdb3Q82/pdb, the X-ray structure of the bacterial receptor with PDB ID 3q82 was obtained. Using a protein preparation module from Auto Dock tools, the receptor structure was altered before being used in the docking investigation. Water molecules close to the protein were removed using techniques for structural refinement. The molecules were drawn in the necessary PDB format. At the binding locations of the receptor structures, each compound was docked. To enhance quality, Discovery Studio 2021 rendered the three-dimensional (3D) structure of each ligand, as well as the receptor and binding interactions. The outcomes of the in-silico molecular docking reveal critical details regarding the potential affinity of the newly designed molecules for the receptor's active areas.

Synthesis

In our previous work^[51] we began with 3,4-dimeth-oxyphenylacetic acid (1) and thiosemicarbazide (2) in POCl₃ and upon conventional heating for over a while was resulted with 5-(3,4-dimethoxybenzyl)-1,3,4-thiadiazol-2-amine (a). In the next step, various Phenacyl bromides (b) were used which gave us the title compounds (3a-3f). To all these derivatives of imidazo[2,1-b] [1,3,4]thiadiazoles Vilsmeyer–Haack reaction was performed for the insertion of the formyl group at the active methyl position (4a-4f). The similar procedures was performed for microwave heating, surprisingly the yields were improved and the formation of unwanted byproducts was significantly reduced with a great reduction in the time of heating. The comparison of the reaction conditions and the yields obtained are indicated in Table 1.

Substrate Scope

For the purpose of assessing the diversity of the synthesised compounds, a thorough analysis was done. The compounds' obtained microwave yields are listed in the substrate scope table. To test whether the reactions could be achieved with microwave heating, different bromoacetophenones were utilised. Different substituents were used in the reactions,

including donating and withdrawing groups. 5-(3,4-dimethoxybenzyl)-1,3,4-thiadiazol-2-amine was combined with different substituted phenacyl bromides to derive the compounds **3(a-f)**. Methoxy and methyl were employed as withdrawing groups, and chloro, bromo, and fluoro were used as donating groups. Furthermore, Vilsmeier-Haack reaction was performed on all of the obtained imidazothiadiazole derivatives to yield 2-(3,4-dimethoxy)-6-(substituted phenyl)- imidazo[2,1-b][1,3,4]thiadiazole-5-carbaldehyde **4(a-f)** as the final resulting compound for the introduction of the formyl group to the imidazo thiadiazole ring. (Scheme 1 and Scheme 2)

Results and Discussion

Chemistry

The present work attributes to the advantages of the microwave method of synthesis over the conventional method. It is supported by the comparison given in Table 1. This novel method of synthesis awards a great reduction in reaction time to improve the yield of title compounds. Also, the ease of handling justified the benefits of this method of synthesis. This study has three steps, the first of which is the production of 5-(3,4-dimethoxybenzyl)-1,3,4-thiadiazol-2-amine. It consists of the calculated and cautious addition of 3,4 dimethoxy phenylacetic acid and thiosemicarbazide to a previously dried microwave glass vial containing POCl₃ as a solvent, which was then irradiated for roughly 20 minutes. TLC was used to monitor the progress of the reaction at 5-minute intervals. The resulting product was purified and examined utilising spectral methods such as mass, IR, and NMR. The mass of the compound was confirmed by the m/z peak at 252.0827. The FT-IR spectra peaks at 3078 and 3261 cm⁻¹ suggested the asymmetric and symmetric absorption bands of -NH2. Using 1H NMR, the structure of 2-amino-1,3,4-thiadiazole was likewise successfully established. The -NH₂ group of the molecule was found to have a singlet at 7.00 ppm.

The second phase in this investigation was the production of 2-(3,4-dimethoxy)-6-(substituted phenyl)-imidazo[2,1-b][1,3,4]thiadiazoles **3(a-f)** in absolute ethanol as a solvent and microwave irradiation at 70 °C for around 30 minutes. The 13C NMR findings show strong evidence for ring cyclization. Peaks between 109 and 111 ppm and 145 and 149 ppm correspond to the C5 and C6 carbons of the cyclized ring. The absence of symmetric and asymmetric -NH2 bands at 3261 and 3078 cm⁻¹

Table 1. Comparison of r	eaction conditions and the yields obtained	d.		
Compound name	Microwave condition (min)	Conventional method (hr)	Yields (%)	
			Microwave	Conventional
a	20	5–6	85	70
3a–3f (6 examples)	30	24	70–85	45–60
4a–4f (6 examples)	10	6-8	70–80	40–55

3.47. Downloaded from https://chemistry-europe.onlinebbrary.wiely.com/doi/10.1002/sl.20.20202877 by University of Mysore, Wiley Online Library on [25/11/2025]. See the Terms and Conditions (https://onlinebbrary.wiely.com/ems-and-conditions) on Wiley Online Library for rules of use; OA articles are governed by the applicable Creative Commons Licensea

Scheme 1. Synthetic route for the synthesis of aldehyde substituted imidazotiadiazoles.

Scheme 2. Substrate scope.

confirms the formation of the fused ring of imidazo[2,1b][1,3,4]thiadiazoles. These findings are also consistent with past research findings.[52]

Formylation of compounds 3(a-f) is the third stage. The Vilsmeyer-Haack reaction was carried out with DMF/POCl₃ as a Vilsmeyer reagent and irradiated at 70-80°C for about 10 minutes to produce the appropriate 2-(3,4-dimethoxy)-6-(substituted phenyl)- imidazo[2,1-b][1,3,4]thiadiazole-5-carbaldehyde 4(a-f). The FT-IR spectrum findings provide critical evidence for the production of formyl group. The aldehyde functional group is represented by the IR absorption band at roughly 1654 cm⁻¹. The production of the formyl group is supported by a singlet at around 10 ppm in 1H NMR and a peak at around 175 ppm in 13C NMR. The supplemental information section contains the analytical data for all the synthesised compounds.

Crystallographic data collection strategy and structure refinement:

The compound **4c**, with the molecular formula C20H16ClN3O3S, crystallises in the monoclinic crystal system with the P21/n space group, according to single crystal X-ray diffraction study. The crystallographic data is stored at the Cambridge Crystallographic Data Centre under the data access

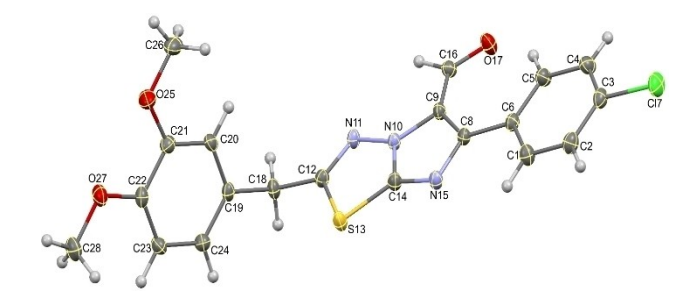


Figure 2. ORTEP of the molecule with thermal ellipsoids drawn at 50% probability.

Table 2. Crystal data and structure re	efinement statistics.
Parameter	value
CCDC deposit No.	CCDC 2184133
Empirical formula	$C_{22}H_{16}CIN_3O_3S$
Formula weight	413.87
Temperature	293 K
Wavelength	0.71075 Å
Crystal system, space group	Monoclinic, $P2_1/n$
Unit cell dimensions	$a = 11.2402(13)$ Å $b = 5.6602(6)$ Å $c = 29.021(4)$ Å $\alpha = 90^{\circ}$ $\beta = 94.042(5)^{\circ}$ $\gamma = 90^{\circ}$
Volume	1841.8(4) ų
Z	4
Density(calculated)	$1.493~{\rm Mg}{\rm m}^{-3}$
Absorption coefficient	0.349 mm^{-1}
F ₀₀₀	856
Crystal size	0.29×0.25×0.23 mm
heta range for data collection	3.63° to 27.50°
Index ranges	$-14 \le h \le 13$ $-7 \le k \le 7$ $-28 \le l \le 37$
Reflections collected	9289
Independent reflections	4122 $[R_{\rm int} = 0.0762]$
Absorption correction	multi-scan
Refinement method	Full matrix least-squares on F ²
Data/restraints/ parameters	4122/0/317
Goodness-of-fit on F ²	1.063
Final [I > 2σ(I)]	R1 = 0.0486, $wR2 = 0.1172$
R indices (all data)	R1 = 0.0571, $wR2 = 0.1243$
Largest diff. peak and hole	0.391 and -0.440 e Å^{-3}

code CCDC 2184133. The ORTEP for the molecule with thermal displacement ellipses created at a 50% probability level is shown in Figure 2. Table 2 covers all of the structure refinement and crystal data information.

Single crystal X-ray diffraction studies confirm the molecular structure of molecule 4c (C22H16CIN3O3S). The list of selected bond lengths, bond angles, and torsion angles is provided in Table S1, Table S2, and Table S3. The bond lengths and bond angles are in good agreement with the typical values. The observed bond distance of C16-O17 is 1.219(2) Å, which is evident for the carbonyl form and consistent with the C=O bond. Similarly, the bond distance of C21-O25 is 1.364(2) Å, C22-O27 is 1.366(2) Å are evident for the C-O bond and are comparable with the standard bond distances. [51,53,54] The structure of the molecule is further described by the torsion angle. The molecule is composed of two phenyl rings with six members and two rings with five members. The eight membered thia-imidazole ring (C8-C9-N10-N11-C12-S13-C14-N15) is formed via the cyclization of the five membered thiadiazole ring (N10-N11-C12-S13-C14) and the five membered imidazole ring (C8-C9-N10-C14-N15). At the meta (C21) and para (C22) locations of one phenyl ring (C19-C20-C21-C22-C23-C24), dimethoxy substituents are present. While a chlorine atom is linked to the other phenyl ring (C1-C2-C3-C4-C5-C6) at the para position (C3). The dihedral angle of 83.99(8)° between the dimethoxy phenyl ring and the thia-imidazole ring proves the molecule's non-planarity. The rings are all planar, with atoms restricted to the same plane and obvious sigplan and sigref values. The aldehyde functional group is substituted at the C9 position of the imidazole ring and is located in the same plane, as evidenced by the torsion angle value of 3.3(4)° around C8-C9-C16-O17. Intermolecular C-H--O interactions and intramolecular C-H--O, C-H--N hydrogen bond interactions stabilise the crystal structure (Table S4).

The molecular structure is also stabilized by C–H··· π , C–Cl··· π and $\pi \cdot \cdot \cdot \pi$ stacking interaction as depicted in the Figure S1, Figure S2 and Figure S3 respectively. The C–H··· π interaction; C(23)-H(23)···Cq4 (Cq4 is the centroid of the ring C19-C20-C21-C22-C23-C24) with a C-Cg distance of 3.717(2) Å, H---Cg distance of 2.85(2) Å, C–H···Cg angle of 149.9(2)° with a symmetry code 5/2-x, 1/2+y, 1/2-z; C(26)-H(26 C)--Cg4 with a C-Cg distance of 3.778(2) Å, H---Cg distance of 2.88(3) Å, C--H---Cg angle of 149(2)° with a symmetry code 1-x, -1+y, z and C(28)-H(28B)···Cg3 (Cg3 is the centroid of the ring C1-C2-C3-C4-C5-C6) with a C-Cg distance of 3.420(2) Å, H---Cq distance of 2.71(2) Å, C--H---Cq angle of $132.1(2)^{\circ}$ with a symmetry code 1/2 + x, 3/2 - y, 1/2 + z. Also, the C(3)-CI(7)--Cg1 (Cg1 is the centroid of the ring N10-N11-C12-S13-C14) with a C-Cg distance of 3.938(2) Å, Cl--Cg distance of 3.407(1) Å, C-Cl--Cg angle of 94.1(7)° with a symmetry code 1-x, 1-y, -z and C(3)-Cl(7)--Cg5 (Cg5 is the centroid of the ring (C8-C9-N10-N11-C12-S13-C14-N15) with a C-Cg distance of 3.626(2) Å, Cl--Cg distance of 3.538(9) Å, C-Cl···Cg angle of 78.71(7)° with a symmetry code 1-x, 1-y, -z.

Similarly, the π -- π interactions; Cg(1)---Cg(2) (Cg(1) is the centroid of the ring N10-N11-C12-S13-C14 and *Cg2* is the centroid of the ring C8-C9-N10-C15-N15) with a *Cg-Cg* distance of 4.0882(1) Å, α =0.94(1)°, β =32.9°, γ =33.1°, a perpendicular



distance of Cg1 (centroid) on Cg2 is 3.4255(7) Å and a symmetry code of 2-x, 1-y, -z; Cg(1)---Cg(5) with a Cg-Cg distance of 3.9618(1) Å, α =0.46(7)°, β =29.8°, γ =30.1°, a perpendicular distance of Cg1 (centroid) on Cg5 is 3.4363(6) Å and a symmetry code of 2-x, 1-y, -z and Cg(2)----Cg(3) with a Cg-Cg distance 3.8530(1) Å, α =4.43(1)°, β =22.4°, γ =25.5°, a perpendicular distance of Cg2 on Cg3 is 3.7851(14) Å and a symmetry code of 1-x, 1-y, -z.

Intermolecular hydrogen bond interactions C–H···O between molecules produce two-dimensional stacking layers through C(18)-H(18)...O(17) As illustrated in Figure S4, and bridged the molecules to form a supramolecular R22(16) ring motif. Furthermore, the C–H··· π , C–Cl··· π , and π ··· π interactions expand the stacking layers to three-dimensional networks, stabilising the compound's crystal structure. When viewed along the a, b, and c axes, respectively, the arrangement of the molecules is shown in Figs. S5, S6, and S7. Blue dotted lines indicate hydrogen bond interactions.

Hirshfeld surface studies

The graphical depiction of the molecular surface is produced as a result of the Hirshfeld surface analysis, which helps to understand the molecular interactions presented by the molecule in the crystalline environment. The Hirshfeld surface was analysed and calculated using the Crystal Explorer 17.5 software using the DFT-B3LYP/6-31G(d,p) basis set. [57–59] The d_{norm} plots were coloured using a scale ranging from $-0.3029\,\mathrm{au}$ (red) to 1.3683 au (blue). The extended 2D fingerprint plots were exhibited in the 0.6–2.8 Å view range, with the de and distance scales shown on the graph axes. The distances to the nearest nuclei outside and inside the surface from the Hirshfeld surface are de and di, respectively. The computed volume inside the Hirshfeld surface is 451.61 ų in a 422.84 Ų area. [58,60-63]

The quantitative contributions of molecular interactions to the overall Hirshfeld surface are determined by analysing the 2D fingerprint plot. The H...H (27.9%) contacts has maximum and O...N (0.1%) has minimum contributions. Similarly, the C... H (21.6%), O...H (15.4%), Cl...H (8.2%), S...H (6.3%), N...H (6.1%), C...C (3.7%), C...N (2.4%), Cl...S (2.1%), C...Cl (1.6%), N...S (1.4%), N...Cl (1.1%), N...N (1%), C...O (0.6%), O...Cl (0.3%) and C...S (0.2%) contacts also contributed to the total area of the surface as shown in Figure S8. Using traditional mapping of d_{norm}, shape index, curvedness, fragment patch, d_e, and di, as shown in Figure S9, these connections are emphasised on the molecular Hirshfeld surface. The many characteristics of the molecular surfaces can be examined using the coloured regions on the surfaces. The shorter and longer intercontacts are indicated on the graph by the red and blue regions, respectively, while the contacts near the van der Waals radii are shown by the white regions. The surface of the negative potential is represented by the red region, and the surface of the positive potential is represented by the blue region. The red triangle concave regions of cyclic stacking contacts and the blue triangle convex sections of the ring atoms of the molecule are represented by the shape index mapped on the Hirshfeld surface, respectively. The C–H···O intermolecular interactions forming $R_2^2(16)$ ring motif is highlighted on d_{norm} Hirshfeld surface of the molecule as shown in Figure S10.

Molecular interaction energy and 3D energy frameworks:

The most effective method, using the Crystal Explorer 17.5 programme, can be used to calculate the molecular interaction energy between compound $4\,c.^{[64,65]}$ By creating a molecular cluster (Figure S11) of radius 3.8 around the chosen molecule $4\,c$, the total interaction energy was calculated. In order to compute the electron densities of the cluster of molecule $4\,c$ that is present around the chosen molecule using the CE-B3LYP/6-31G(d,p) energy model with the scale factors to determine Etot, molecular wave functions were generated using symmetry operations. $K_{ele} = 1.057$, $K_{pol} = 0.740$, $K_{dis} = 0.871$, $K_{rep} = 0.618$.

Table S5 lists the crystallographic symmetry operations and the molecular interaction energies associated with them (where R is the separation between molecular centroids (mean atomic position) in and N is the quantity of molecules at that separation; energies are in kJ mol⁻¹). The highest total interaction energy was displayed by the sky-blue coloured molecule with symmetry operation (-x, (-y, (-z)) at a distance of 6.08 Å from the centroid of the chosen molecule, while the lowest total interaction energy was displayed by the dark blue coloured molecule with symmetry operation (x + 1/2, -y + 1/2, z+ 1/2) at a distance of 14.14 Å from the centroid of the chosen molecule. The energy frameworks were built using the molecular pair interaction energy calculations to determine the total interaction energy (-262.07 kJ mol⁻¹), which included the electrostatic $(-96.40 \text{ kJ} \text{ mol}^{-1})$, polarisation $(-19.90 \text{ kJ} \text{ mol}^{-1})$, dispersion ($-287.78 \text{ kJ} \text{mol}^{-1}$), and repulsion ($142.02 \text{ kJ} \text{mol}^{-1}$) energies. The compound's energy frameworks for electrostatic, dispersion, and total energy terms were constructed, and they were displayed as variously coloured cylinders with scale factors (cylinder tube sizes) of 100 and cutoff energies of -50 kJ/mol. These cylinders show the strength of the molecular packing in various orientations as well as the size of the interaction energy between molecule pairs. The molecular cluster's red cylinders stand in for electrostatic energy (E_{elec}), while the green and blue cylinders represent dispersive and total interaction energies, respectively. (Figure \$12). According to the energy framework calculations, the molecules' dispersion energy in a crystalline environment outweighs their electrostatic and polarisation energies. By creating the molecular cluster with a radius of 25 Å, the calculations for molecular energy were expanded. The molecular cluster is depicted in Figs. S13, S14, and S15 along the a, b, and c axes, respectively. It is discovered that the compound 4c has a lattice energy of $-266.9 \text{ kJ} \text{ mol}^{-1}$. [66]



Quantum chemical calculations, frontier molecular orbitals and natural bond orbitals

To comprehend the electrical and chemical features of the complex, quantum chemical calculations, analysis of the border molecular orbitals, atomic charges, and surface investigations are crucial. By doing DFT calculations with the Gaussian16 programme, B3LYP hybrid functional, and 6-311+G(d,p) basis set in gas phase, the compound's molecular coordinates were optimised. Figure 3 depicts the molecule 4c's optimised structure. The correlation coefficients (CC) for bond lengths (0.9981), bond angles (0.9958), and torsion angles (0.9998) are listed in Tables S1, S2, and S3, respectively, and they demonstrate the strong agreement between the theoretically predicted and experimentally determined values.

Additionally, Table S6 includes the calculated and tabulated energies of the frontier molecular orbitals (HOMO-LUMO), the energy band gap (E gap), the ionisation potential (I), the electron affinity (A), the absolute electronegativity (χ), the global hardness (η), the global softness (σ), the global electrophilicity (ω), the chemical potential (μ), and the dipole moment (D). [67-69] Figure 4 displays the HOMO and LUMO energy map together with the band gap energies.

Each atom's mulliken charges were determined by the DFT calculation (Table S7 and Figure S16). When compared to other hydrogen atoms, the hydrogen atoms bonded to the methoxy



Figure 3. DFT optimized structure of compound 4 c.

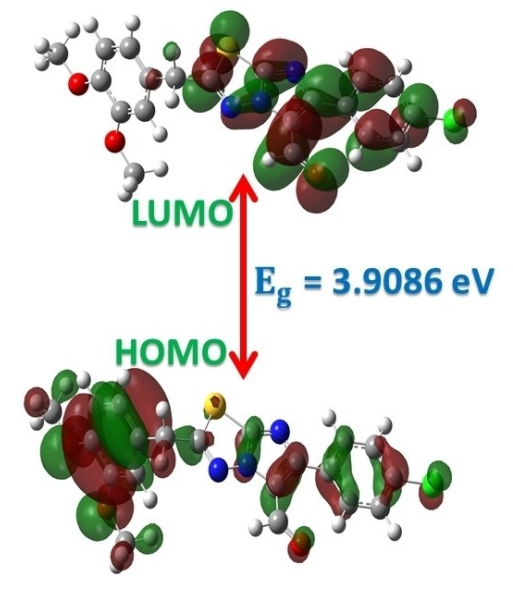


Figure 4. Frontier molecular orbitals of compound 4c.

carbon atom have large positive atomic charges. Only a few carbon atoms and oxygen atoms have demonstrated negative charges, and they connect with the positively charged acceptors with ease. Due to the atoms in its immediate surroundings, the C19 (0.9929) atom displayed the most electro-positivity, whereas the C21 (-0.7165) atom displayed the highest electronegativity. Figure S17 displays the compound's molecular electrostatic potential (MEP) map, which was produced using a colour scale with values ranging from -4.959 e⁻² au (deepest red) to $+4.959 e^{-2}$ au (deepest blue). The charge distribution on the molecular surface is represented by the study of the MEP surface. The coloured area on the surface served as a marker for the chemically reactive areas. MEP's positive sections (blue) signify electrophilicity, while its negative parts (green) connect to the molecule's nucleophilicity and its red regions, its electrophilic character. According to the MEP analysis, the methoxy functional groups of compound 4c's nucleophilic negative regions are dispersed around the oxygen atoms, while the electrophilic blue regions are concentrated around the hydrogen atoms connected to the carbon atoms.

in-silico docking results

We chose to conduct in-silico molecular docking experiments on the antibacterial 3g82 receptor in order to understand the binding interactions of synthetic drugs on antibacterial activity. 3q82 is Meropenem acylated BlaR1 sensor domain from Bacillus subtilis and the expression system is Escherichia coli. The drug of choice was chloramphenicol, which is a HYDROLASE REGULATOR/ANTIBIOTIC. The stability of the best-docked pose of these compounds was examined by analyzing the hydrogen bonding interactions of the protein with these compounds, which identified the amino acids involved in hydrogen bond formation. Based on these dynamics, 4f (Figure 5) has the lowest binding scores of -8.9 Kcal/mol compared to conventional chloramphenicol (-7.3 Kcal/mol), as reported in Table 3. The compounds 4(a-f) demonstrate a variety of binding interactions (hydrogen bonding, π - π , π -Alkyl) with various amino acid residues found in the receptor enzymes (3q82), resulting in the compound 4f producing an ideal binding species for the antibacterial receptor. The typical hydrogen bonding between the molecules are depicted in 2D images. In

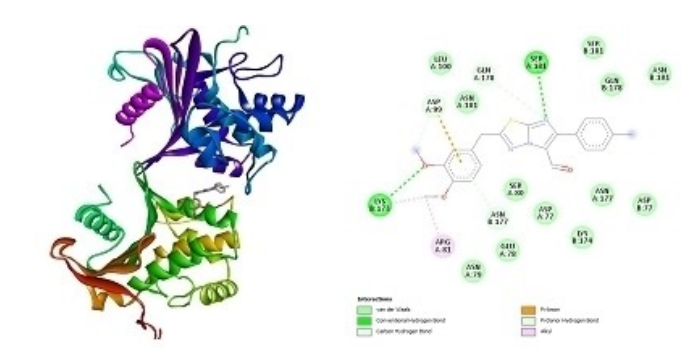


Figure 5. Different modes of binding interaction of **4f** with receptor 3Q82: 3D interaction and 2D interaction.



Table 3. Docking scores.		
Compound	Receptor	Docking Score (Kcal/mol)
4a	3q82	-8.6
4 b	3q82	-8.7
4c	3q82	-8.7
4 d	3q82	-8.6
4 e	3q82	-8.7
4f	3q82	-8.9
CHLORAMPHENICOL	3q82	-7.3

molecule **4f**, the usual hydrogen is joined to the oxygen of the methoxy group and the nitrogen of the imidazole ring. The lengths are, respectively, 4.73 and 4.31. The theoretical hydrogen bond distances and these bond lengths accord fairly well. The **4(a–f)** interaction (π - π , π -Alkyl) with active sites of Meropenem acylated BlaR1 sensor with amino acid residues are ASP77, ASN101, MET165, LYS173, LYS176, ASN177, SER180, SER181, TYR194, TYR214,TYR221. The optimal docking, two-dimensional, and three-dimensional bonding orientations for, **4a**, **4b**, **4c**, **4d**, **4e**, **4f** and chloramphenicol are denoted by S18, S19, S20, S21, S22, S23 and S24 respectively.

Biological activities

Antibacterial Assay

The disc diffusion method was used to assess the antibacterial activity of all the final step compounds (4a, 4b, 4c, 4d, 4e, and 4f). E. coli and B. subtilis were the bacteria strains that were employed. Before usage, stock cultures of bacteria were kept at 40 °C on the slant of Nutrient agar (NA). All samples' antibacterial activity was assessed using the Whatman No. 1 paper disc diffusion method.^[70] Each of the bacteria acquired nutrient agar plates. The test was conducted using 5 mmdiameter discs. To the discs, 200 µg of concentrate was added. Dried discs were positioned on plates that had already been infused with a bacterial slurry that contained 1X106 cfu/ml. Chloramphenicol commercial antibiotic discs with a 10 µg concentration were utilised as a benchmark for antibacterial activity. Three replicates for each treatment were collected. The zones of inhibition were determined by comparing the plates to the reference antibiotic (chloramphenicol 110 µg/disc) after the plates had been incubated at 37 °C for 24 hours. A zone below 4 mm was regarded as resistant (R), a zone of 6 mm and above as highly sensitive (HS) to the test material, and a zone of 4-5 mm as moderately sensitive (MS). (Table 4)

Minimal Inhibitory Concentration (MIC)

MIC was determined using the broth microdilution assay as described by^[71] with slight modification. Minimum inhibitory concentrations (MIC) of 4a, 4b, 4c, 4d, 4e, and 4f was

Table 4. Antibacterial activ	vity of the 4(a–f) compo	ounds.
Samples Concentration of the	Microorganism Zone of inhibition i	n mm
samples 100 μg/ml	Gram negative bacteria (<i>E.coli</i>)	Gram positive bacteria (B.subtilis)
Chloramphenicol	26.25 ± 0.87	25.45 ± 0.32
4a	08.56 ± 0.76	10.33 ± 0.54
4 b	09.23 ± 0.66	08.64 ± 0.32
4c	11.64 ± 0.78	10.54 ± 0.11
4 d	06.43 ± 0.89	09.21 ± 0.37
4 e	06.76 ± 0.34	$\textbf{04.55} \pm \textbf{0.67}$
4f	09.22 ± 0.65	11.67 ± 0.96

The value of $p \le 0.05$ was considered statistically significant. Negative (–) sign indicate no inhibition

determined using B.subtilis (gram-positive bacteria) and E. coli (gram-negative bacteria). To dilute mid-logarithmic phase cells, 0.1 M sodium phosphate buffer, pH 7.4, was utilised. Each well of 96-well propylene microtitre plates received 10 μ L of serially diluted test samples with concentrations ranging from 5 to 200 μ g/mL. The plates were incubated at 37 °C for 24 hours. The controls were carried out similarly but without the test samples. By measuring absorbance at 595 nm in a microtitre plate reader using multiskan Go software, growth inhibition was identified. The lowest concentration, or MIC, was noted since there was no discernible growth in the broth. The studies were performed in triplicate, and the MIC was determined by averaging the results of three separate trials. (Table 5)

Antioxidant assay

Determination of hydroxyl radical scavenging activity by 2-Deoxy D-ribose assay

The 2-Deoxy D-ribose assay was used to test the hydroxyl radical scavenging capacity of compounds **4a**, **4b**, **4c**, **4d**, **4e**, and **4f**. FeCl3 (100 μ M), ascorbate (100 μ M), EDTA (104 μ M), H2O2 (1 mM), and 2-deoxy-D-ribose (2.8 mM) were added to a reaction mixture together with 100 μ g of each peak fraction

Table 5. N	linimum Inhibitory Concentrat	ion (MIC) of the compounds.
Samples	Microorganism MIC in μg	
	Gram negative bacteria (E.coli)	Gram positive bacteria (<i>B.sub-tilis</i>)
4a	60 ± 0.54	50±0.67
4 b	65 ± 0.89	$60\pm.33$
4 c	40 ± 0.97	40 ± 0.54
4 d	80 ± 0.54	60 ± 0.54
4 e	100 ± 0.89	100 ± 0.89
4f	40±0.97	40±0.97

Europe

(AS1 and AS2) in a 20 mM potassium phosphate buffer at a pH of 7.4 before being incubated for one hour at 37 °C. A known antioxidant, such as reduced glutathione, was utilised as the positive control in a comparable experiment. The reaction mixture was heated at 95°C in a boiling water bath for 15 minutes after adding 1 ml of TBA (0.5%). At 535 nm, the optical density of the reaction mixture was measured after it had been cooled on ice. The right controls and blanks were used for the test. The amount of inhibition of the generation of hydroxyl radicals used to measure antioxidant activity. The same protocol was followed for the peak fractions (P1-P4) obtained from preparative rp-HPLC (Figure 6).

Hydroxyl radical scavenging activity
$$(\%) =$$
 A blank – A sample
$$= -X \ 100 \label{eq:10}$$

1, 1-diphenyl-2-picrylhydrazyl (DPPH) radical scavenging activity

1, 1-diphenyl-2-picrylhydrazyl (DPPH) radical scavenging activity was assessed according to the reported method with few modifications. [72,73] 20 μg of each of the compounds (4a, 4b, 4c, 4d, 4e, and 4f) were added to the reaction mixture together with 1 ml of a freshly prepared 0.5 mM ethanolic DPPH solution and 2.0 ml of 0.1 M acetate buffer, pH 5.5. Quercitin at a 20µg concentration was used as a positive control in a similar experiment. The resulting solutions were then left to stand at 37 °C for 30 min, the reading was recorded at 517 nm in Hitachi U-2900 spectrophotometer (As) as absorbance of the tested sample. Higher DPPH scavenging activity is represented by lower absorbance at 517 nm. Along with the necessary buffer, a uitable Blank test or control (Ac) was also taken. By comparing the inhibition percentage to the control, the calculation was done. Antioxidant activity was measured as a percentage of reduced DPPH radical generation. (Figure 7)

DPPH radical scavenging activity
$$(\%) = Ac-As/AcX1$$
 (2)

Haemolysis assay: With a small modification, hemolytic activity was measured in accordance with Jang et al.'s instructions. In a nutshell, isotonic PBS, pH 7.4, was used to wash 5 ml of freshly produced human blood cells (RBCs) until the colour of the supernatant became colourless. The same buffer was then used to dilute the cleaned RBCs to a final volume of 30 ml. 20 µg of the compound from each series (4a, 4b, 4c, 4d, 4e and 4f) was added to 190 μl of the cell suspension in microfuge

Sample	Mean
Quercitin	92 ± 0.87
4a	86 ± 0.01
4b	75 ± 0.83
4c	69 ± 0.20
4d	54 ± 0.17
4e	68 ± 0.17
4f	60 ± 0.38

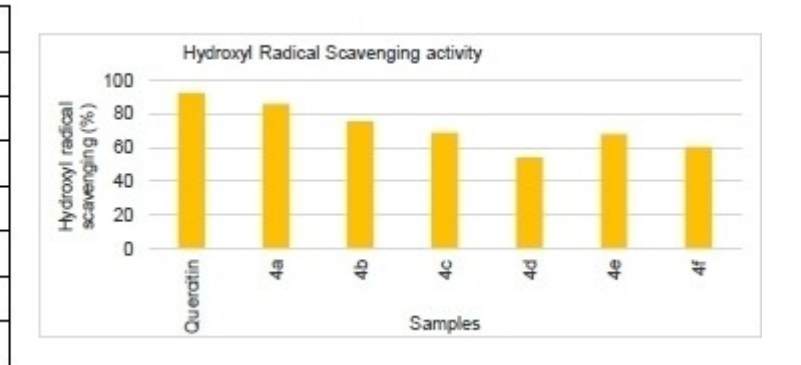


Figure 6. Representation of Hydroxyl Radical Scavenging Activity.

Sample	Mean (%)
Quercitin	97 ± 0.34
4a	71 ± 0.96
4b	66 ± 0.23
4c	62 ± 0.08
4d	40 ± 0.27
4e	67 ± 0.94
4f	59 ± 0.25

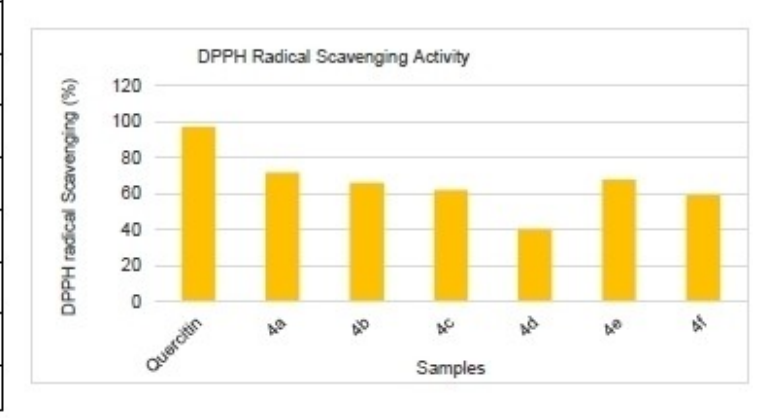


Figure 7. Representation of DPPH Radical Scavenging Activity.

3, 47, Downloaded from https://chemistry-europe.onlinelibrary.wiley.com/doi/10.1002/slct.202302877 by University of Mysore, Wiley Online Library on [25/11/2025]. See the Terms and Conditions (https://onlinelibrary.wiley.com/ems-and-conditions) on Wiley Online Library for rules of use; OA articles are governed by the applicable Creative Commons Licensean Conditions (https://onlinelibrary.wiley.com/ems-and-conditions) on Wiley Online Library for rules of use; OA articles are governed by the applicable Creative Commons Licensean Conditions (https://onlinelibrary.wiley.com/ems-and-conditions) on Wiley Online Library for rules of use; OA articles are governed by the applicable Creative Commons Licensean Conditions (https://onlinelibrary.wiley.com/ems-and-conditions) on Wiley Online Library for rules of use; OA articles are governed by the applicable Creative Commons Licensean Conditions (https://onlinelibrary.wiley.com/ems-and-conditions) on Wiley Online Library for rules of use; OA articles are governed by the applicable Creative Commons Licensean Conditions (https://onlinelibrary.wiley.com/ems-and-conditions) on Wiley Online Library for rules of use; OA articles are governed by the applicable Creative Commons Licensean Conditions (https://onlinelibrary.wiley.com/ems-and-conditions) on Wiley Online Library for rules of use; OA articles are governed by the applicable Creative Commons (https://onlinelibrary.wiley.com/ems-and-conditions) on the article of the

tubes. Gently combining the contents, incubating them at $37\,^{\circ}\text{C}$ for 30 minutes, and centrifuging them for 5 minutes at 4000 g. In order to track the release of haemoglobin, which is an indicator of membrane damage, aliquots of $150\,\mu\text{l}$ of the supernatant were diluted to 1 ml with PBS and the absorbance was measured at 567 nm. PBS and Triton X 100 were found to have zero hemolysis and $100\,\%$ lysis, respectively. The following equation was used to determine the proportion of hemolysis. (Figure 8)

Haemolysis
$$(\%) = (A_s - A_c)/(A_{100} - A_0) \times 100$$
 (3)

Where, A_s is the absorbance of the sample, A_{100} is the absorbance of the completely lysed RBCs in 0.2% Triton X-100 and A_0 is the absorbance in the complete absence of haemolysis

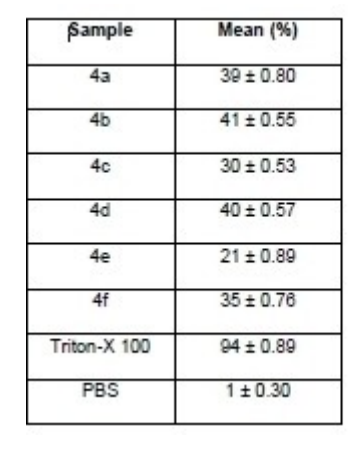
Conclusions

A series of aldehyde substituted imidazothiadiazole were synthesized using microwave irradiation technique in comparison with the conventional method of heating. Spectroscopic techniques such 1H NMR, 13C NMR, mass spectroscopy, and FT-IR were used to predict the structures. The facts obtained and the expected structures and literature sources correlate fairly well. Single crystal X-ray diffraction experiments were used to identify the crystal structure of compound 4c. The compound crystallized in a monoclinic crystal system under the P2₁/n space group. The molecular structure is stabilized by intermolecular C-H...O and intramolecular C-H...O, C-H...N hydrogen bond interactions. The crystal structure also exhibits intermolecular C–H... π , C–Cl... π and π ... π stacking interactions. Using fingerprint plots and Hirshfeld surface analyses, the intermolecular interactions are measured. 3D D_{norm} surfaces were used to investigate the surface characteristics. The calculations for the energy frameworks showed that the dispersion energy (-287.78 kJ/mol) outweighs all other energies. The molecule's lattice energy is determined to be -266.9 kJ/mol. The electrical characteristics of the molecule were also calculated using the density functional theory. It is discovered that the HOMO-LUMO energy gap is 3.9086 eV. Finally, the chemically active regions on the molecule are identified by analysing the molecular electrostatic potential map. The compound 4f exhibited more negative values (-8.9 kcal/mol) than the standard chloramphenicol (-7.3 kcal/mol) in docking studies. Supporting this data, the compounds were evaluated for their antibacterial activity. When compared to chloramphenicol, the compounds 4a, 4b, 4c, and 4f showed modest antibacterial activity, with a zone of inhibition of between 9 mm and 11 mm in diameter at a concentration of 100 µg/ml. Minimum Inhibitory Concentration was evaluated in between 40-70 μg/ml. Free radical scavenging activity was determined by two different assays. The per cent scavenging activity was 60-85% and 40-70% for hydroxyl free radical scavenging activity and DPPH radical scavenging activity respectively. Per cent, hemolysis activity or cell protective activity of the compounds was rather ineffective with 20-40%.

Experimental

Synthesis of 5-(3,4-dimethoxybenzyl)-1,3,4-thiadiazol-2-amine (a):

4-5 ml of POCl3 were poured into a G-30 glass vial that has a snap cap and a magnetic bit. It was kept at an ice-cold temperature. Thiosemicarbazide (0.15 mol) and 2-(3,4-dimethoxyphenyl)acetic acid (0.1 mol) were accurately weighed and thoroughly combined. The combined contents were put into a microwave glass vial that was kept at a very cold temperature. After that, the vial was placed in the heating chamber of the microwave apparatus and exposed to radiation for 20 minutes at 80 °C. With the aid of an air compressor linked to the heating cavity, the glass vial was allowed to cool to room temperature inside the instrument. The reaction mixture was poured into ice cold water and ammonia was added to the vial's contents to make them basic. The obtained precipitate was filtered, water washed, and thoroughly dried.



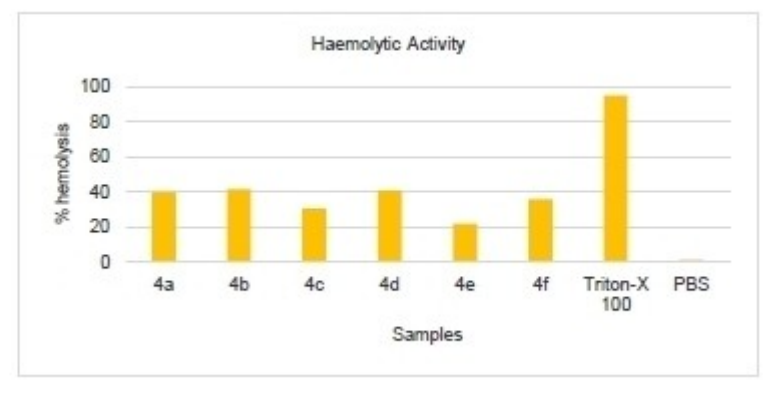


Figure 8. Representation of Haemolytic Activity.



General procedure for the preparation of 2-(3,4-dimethoxy)-6-(substituted phenyl)- imidazo[2,1-b][1,3,4]thiadiazoles 3(a-f):

5-(3,4-dimethoxybenzyl)-1,3,4-thiadiazol-2-amine (0.1 mmol) and different bromo acetophenones (0.1 mmol) were introduced to a G-30 glass vial with a snap cover and a magnetic bit while using ethanol as the solvent (15 ml). At 70 °C, the reaction mixture was exposed to radiation for roughly 30 minutes. TLC was observed on a regular basis every 10 minutes. With the aid of an air compressor linked to the heating cavity, the glass vial was allowed to cool to room temperature inside the instrument. It was possible to obtain solid hydro bromide salt, which was then filtered out, lightly rinsed with cold ethanol, and thoroughly dried. A cold sodium carbonate aqueous solution was used to treat the residue. Furthermore, dichloromethane (2×20 mL) was used to extract the free base. Crystals were grown using a slow evaporation technique using ethyl acetate as a solvent over a period.

General procedure for the preparation of 2-(3,4-dimethoxy)-6-(substituted phenyl)- imidazo[2,1-b][1,3,4]thiadiazole-5-carbaldehyde 4(a-f):

The Vilsmeier-Haack reagent was made by adding POCI3 (16 mmol) dropwise to swirling dimethylformamide (10 ml) kept at ice-cold conditions in a G-30 glass vial with a snap cover and magnetic bit. The aforementioned reagent was combined with 5-mmol of 2-(3,4 $dimethoxy) \hbox{-6-(substituted $phenyl)$-imidazo $[2,1-b]$ $[1,3,4]$ thiadiazole,}$ and stirring was carried out for an additional two hours. The vial was moved to the heating chamber of the microwave apparatus and exposed to radiation for 10 minutes at 90 °C. With the aid of an air compressor linked to the heating cavity, the glass vial was allowed to cool to room temperature inside the instrument. The resultant reaction mixture was added to 100 ml of water, and the precipitate was filtered before being suspended in water and adjusted to pH 7 using a cold sodium carbonate aqueous solution. Utilising, the isolated solid was separated. Ethyl acetate was used as the solvent for the slow evaporation procedure used to form the crystals, which were then left at room temperature unaltered.

Crystallographic data

Deposition Number 2184133 (for 4c) contain the supplementary crystallographic data for this paper. These data are provided free of charge by the joint Cambridge Crystallographic Data Center and Fachinformationszentrum Karlsruhe Access Structures service www.ccdc.cam.ac.uk/structures.

Supporting Information Summary

Details of the experimental methods (synthetic, biological, and theoretical) are provided in the supporting information, together with spectral characterisation data for each compound (1H NMR, 13C NMR, FT-IR).

Acknowledgements

Sagar K.S. thank DBT-Glue grant project (NO. BT/PR23078/MED/29/1253 dated: 22.03.2018), VGST Project (No. KSTePS/VGST/GRD-681/KFIST(L1)/2018 dated 27.08.2018) DST-Ph.D. fellowship (Award No. DST/KSTePS/Ph.D. Fellowship/CHE-03.2021-22/1213

dated 09.01.2023) for the financial support. Authors are grateful to the IOE, Vijnana bhavan, University of Mysore, Mysuru for instrumentation facilities, National Single Crystal Diffractometer Facility, DOS in Physics, University of Mysore for providing X-ray diffraction data.

Conflict of Interests

The authors declare no conflict of interest.

Data Availability Statement

The data that support the findings of this study are available from the corresponding author upon reasonable request.

Keywords: antioxidant assay \cdot crystallography \cdot DFT calculations \cdot in-silico studies \cdot microwave-assisted synthesis

- [1] M. Gaba, N. Dhingra, Indian J. Pharm. Educ. 2011, 45, 175–183.
- [2] R. Cerón-Camacho, J. A. Aburto, L. E. Montiel, R. Martínez-Palou, Comptes Rendus Chim. 2013, 16, 427–432.
- [3] R. Subramaniyan, R. Ramarajan, A. Ramalingam, S. Sambandam, A. Petersamy, A. R. Guerroudj, N. Boukabcha, A. Chouaih, J. Mol. Struct. 2023, 1278, 134946.
- [4] F. A. Bassyouni, S. M. Abu-Bakr, M. A. Rehim, Res. Chem. Intermed. 2012, 38, 283–322.
- [5] N. C. S. Srinivas cheruku, Yateesh Narayana, Makanahalli P. Sunil kumar, Manikya Kumara, Kanchagarakoppal S. Rangappa, Kempegowda Mantelingu, New J. Chem. 2022,46, 4421–4426.
- [6] C. Duangkamol, P. Batsomboon, A. E. Stiegman, G. B. Dudley, Chem. An Asian J. 2019, 14, 2594–2597.
- [7] S. Shamanth, N. Chaithra, M. Gurukiran, M. Mamatha, N. K. Lokanath, K. S. Rangappa, K. Mantelingu, Org. Biomol. Chem. 2020, 18, 2678–2684.
- [8] L. Kumar, S. S. Tabassum, S. K S. S. Govindaraju, ChemistrySelect. 2022, 7, e202203668.
- [9] M. B. Gawande, S. N. Shelke, R. Zboril, R. S. Varma, Acc. Chem. Res. 2014, 47, 1338–1348.
- [10] J. Shah, K. Mohanraj, Indian J. Pharm. Sci. 2014, 76, 46–53.
- [11] U. Ray, V. K. Gopinatha, S. Sharma, L. Goyary, B. Choudhary, K. Mantelingu, K. S. Rangappa, S. C. Raghavan, FEBS J. 2023, 290, 796–820.
- [12] J. Khalafy, N. Etivand, N. Khalillou, Heterocycl. Commun. 2018, 24, 297–302.
- [13] T. Eysteinsson, H. Gudmundsdottir, A. O. Hardarson, E. Berrino, S. Selleri, C. T. Supuran, F. Carta, Int. J. Mol. Sci. 2019, 20, 1–12.
- [14] P. W. Jones, M. Greenstone, *Cochrane database Syst. Rev.* **2001**, CD002881.
- [15] D. Wile, Ann. Clin. Biochem. 2012, 49, 419–431.
- [16] R. Kumar, V. Sharma, S. Bua, C. T. Supuran, P. K. Sharma, J. Enzyme Inhib. Med. Chem. 2017, 32, 1187–1194.
- [17] A. K. Jain, S. Sharma, A. Vaidya, V. Ravichandran, R. K. Agrawal, Chem. Biol. Drug Des. 2013, 81, 557–576.
- [18] U. Ray, S. K. Raul, V. K. Gopinatha, D. Ghosh, K. S. Rangappa, K. Mantelingu, S. C. Raghavan, *Mol. Carcinog.* 2020, *59*, 618–628.
- [19] T. Jabeen, S. Aslam, M. Yaseen, M. Jawwad Saif, M. Ahmad, S. A. Al-Hussain, M. E. A. Zaki, J. Saudi Chem. Soc. 2023, 27, 101679.
- [20] K. F. M. Atta, O. O. M. Farahat, A. Z. A. Ahmed, M. G. Marei, *Molecules*. 2011, 16, 5496–5506.
- [21] B. Sharma, A. Verma, S. Prajapati, U. K. Sharma, *Int. J. Med. Chem.* **2013**, 1–16.
- [22] V. B. Jadhav, M. V. Kulkarni, V. P. Rasal, S. S. Biradar, M. D. Vinay, Eur. J. Med. Chem. 2008, 43, 1721–1729.
- [23] M. A. Syed, Y. Reddy, P. Reddy, K. B. Chandrasekhar, **2018**, *8*, 21–27.
- [24] G. Mazzone, F. Bonina, A.M. Panico, G. Puglisi, G. Marchetta, M. Amico Roxas, A. Caruso, G. Blandino, Farmaco Ed. Sci. 1984, 39, 585–598.
- [25] A. Marin, N. Valls, F. J. Berenguer, M. T. Alonso, A. Ramon Martinez, M. Mercedes Martinez, J. Elguero, Farmaco 1992, 47, 63–75.



- [26] I. A. Khazi, C. S. Mahajanshetti, A. K. Gadad, A. D. Tarnalli, C. M. Sultanpur, Arzneimittelforschung. 1996, 46, 949–952.
- [27] M. A. el-Sherbeny, E. R. el-Bendary, H. I. el-Subbagh, H. A. el-Kashef, Boll. Chim. Farm. 1997, 136, 253–256.
- [28] A. Tahghighi, F. Babalouei, Iran. J. Basic Med. Sci. 2017, 20, 613–622.
- [29] A. Ergena, Y. Rajeshwar, G. Solomon, Scientifica (Cairo). 2022, 3011531.
- [30] X. Ding, Z. Zhai, L. Lv, Z. Sun, X. Liu, Front. Chem. Sci. Eng. 2017, 11, 379–386.
- [31] V. Gopalakrishnan, S. Sharma, U. Ray, M. Manjunath, D. Lakshmanan, S. V Vartak, V. K. Gopinatha, M. Srivastava, M. Kempegowda, B. Choudhary, S. C. Raghavan, Mol. Carcinog. 2021, 60, 627–643.
- [32] R. N. Suresh, T. R. Swaroop, D. Gowda, K. Mantelingu, K. S. Rangappa, RSC Adv. 2023, 13, 4910–4916.
- [33] S. Cheruku, A. M. Sajith, Y. Narayana, P. Shetty, S. C. Nagarakere, K. S. Sagar, K. N. Manikyanally, K. S. Rangappa, K. Mantelingu, J. Org. Chem. 2021, 86, 5530–5537.
- [34] S. Shamanth, S. C. Nagarakere, K. S. Sagar, Y. Narayana, M. Mamatha, K. S. Rangappa, M. Kempegowda, *Synth. Commun.* **2021**, *51*, 1197–1205.
- [35] S. Shamanth, N. C. Sandhya, Y. Narayana, S. Makanahalli, P. M. Mamatha, K. S. Rangappa, M. Kempegowda, Synth. Commun. 2022, 52, 1122–1130.
- [36] S. Ramkumar, R. Ramarajan, R. Rajalakshmi, R. Subramaniyan, R. Ramarajan, A. Ramalingam, S. Sambandam, A. Petersamy, A. R. Guerroudj, N. Boukabcha, A. Chouaih, N. D. kumar, P. Mayavel, I. Muthuvel, G. Thirunarayanan, Chem. Data Collect. 2023, 8, e202204494.
- [37] Kemparajegowda, H. A. Swarup, S. Chandrasekhar, B. K. Jayanna, K. Kumara, N. K. Lokanath, S. B. Thimmaiah, K. Mantelingu, J. Mol. Struct. 2022, 1251, 131970.
- [38] T. S. Shashidhara, C. S. Navyashree, M. K. Hema, K. Mantelingu, R. J. Ramalingam, M. Karnan, M. Umashankar, N. K. Lokanath, J. Mol. Struct. 2023, 1293, 136266.
- [39] T. N. Lohith, S. Shamanth, M. A. Sridhar, K. Mantelingu, N. K. Lokanath, J. Mol. Struct. 2022, 1252, 132203.
- [40] Mahesha, T. C. Raveesha, M. K. Hema, K. J. Pampa, P. G. Chandrashekara, K. Mantelingu, T. Demappa, N. K. Lokanath, J. Mol. Struct. 2021, 1225, 129104
- [41] K. M. Chandini, T. N. Lohith, S. Shamanth, M. A. Sridhar, K. Mantelingu, N. K. Lokanath, J. Mol. Struct. 2023, 1283, 135320.
- [42] N. D. kumar, P. Mayavel, I. Muthuvel, G. Thirunarayanan, Chem. Data Collect. 2020, 30, 100547.
- [43] S. Ramkumar, R. Ramarajan, ChemistrySelect 2023, 8, e202204494.
- [44] A. S. Zarena, S. Gopal, R. Vineeth, J. Anal. Methods Chem. 2014, 989543.
- [45] K. Amin, R.-M. Dannenfelser, J. Pharm. Sci. 2006, 95, 1173-1176.
- [46] CrystalClear, Rigaku/MSC, Inc, New Trails Drive, Woodlands, TX 77381.2005, 9009.
- [47] G. M. Sheldrick, Acta Crystallogr. Sect. A Found. Crystallogr. 2008, 64, 112–122.
- [48] A. L. Spek, J. Appl. Crystallogr. 2003, 36, 7–13.
- [49] C. F. MacRae, I. Sovago, S. J. Cottrell, P. T. A. Galek, P. McCabe, E. Pidcock, M. Platings, G. P. Shields, J. S. Stevens, M. Towler, P. A. Wood, J. Appl. Crystallogr. 2020, 53, 226–235.
- [50] K. Gowda, H. A. Swarup, S. C. Nagarakere, S. Rangappa, R. S. Kanchugarkoppal, M. Kempegowda, Synth. Commun. 2020, 50, 1528–1544.

- [51] K. S. Sagar, S. Shamanth, K. Kumara, N. K. Lokanath, K. Mantelingu, M. N. Kumara, Chem. Data Collect. 2022, 42, 100962.
- [52] M. Dagli, M. Er, T. Karakurt, A. Onaran, H. Alici, H. Tahtaci, ChemistrySelect 2020, 5, 11753–11763.
- [53] K. Kumara, A. Dileep Kumar, S. Naveen, K. Ajay Kumar, N. K. Lokanath, J. Mol. Struct. 2018, 1161, 285–298.
- [54] K. Kumara, A. Dileep Kumar, S. Naveen, K. Ajay Kumar, N. K. Lokanath, J. Mol. Struct. 2018, 1161, 285–298.
- [55] J. Bernstein, R. E. Davis, L. Shimoni, N.-L Chang, Angew. Chem. Int. Ed. Engl. 1995, 34, 1555–1573.
- [56] K. Kumara, N. Shivalingegowda, L. D. Mahadevaswamy, A. K. Kariyappa, N. K. Lokanath, Chem. Data Collect. 2017, 9–10, 251–262.
- [57] J. J. McKinnon, D. Jayatilaka, M. A. Spackman, Chem. Commun. 2007, 1, 3814–3816.
- [58] P. Manna, S. K. Seth, M. Mitra, A. Das, N. J. Singh, S. R. Choudhury, T. Kar, S. Mukhopadhyay, CrystEngComm. 2013, 15, 7879–7886.
- [59] P. R. Spackman, M. J. Turner, J. J. McKinnon, S. K. Wolff, D. J. Grimwood, D. Jayatilaka, M. A. Spackman, J. Appl. Crystallogr. 2021, 54, 1006–1011.
- [60] V. Channa Basappa, V. Hamse Kameshwar, K. Kumara, D. K. Achutha, L. Neratur Krishnappagowda, A. K. Kariyappa, Heliyon 2020, 6, e05290.
- [61] Lohith T. N, Hema M. K, Karthik C. S, Sandeep S, Mallu P, Jothi R. R, Sridhar M. A, M. Karnan, Loknath N. K, J. Mol. Struct. 2022, 1267, 133476.
- [62] A. L. A. Kala, K. Kumara, N. V. Harohally, N. K. Lokanath, J. Mol. Struct. 2020, 1202, 127238.
- [63] A. H. Udaya Kumar, Mahesha, K. J. Pampa, K. Kumara, M. K. Hema, N. V. Harohally, N. K. Lokanath, J. Mol. Struct. 2022, 1265, 133409.
- [64] K. Kumara, M. Jyothi, S. Kouser, A. H. U. Kumar, I. Warad, S. A. Khanum, N. K. Lokanath, J. Mol. Struct. 2023, 1272, 134226.
- [65] M. W. Shi, S. P. Thomas, G. A. Koutsantonis, M. A. Spackman, Cryst. Growth Des. 2015, 15, 5892–5900.
- [66] R. Kumar, R. Kamal, V. Kumar, J. Parkash, J. Mol. Struct. 2022, 1250,
- [67] S. Xavier, S. Periandy, S. Ramalingam, Spectrochim. Acta Part A 2015, 137, 306–320.
- [68] I. Warad, F. F. Awwadi, M. Daqqa, A. Al Ali, T. S. Ababneh, T. M. A. AlShboul, T. M. A. Jazzazi, F. Al-Rimawi, T. Ben Hadda, Y. N. Mabkhot, J. Photochem. Photobiol. B 2017, 171, 9–19.
- [69] Y.-X. Sun, Q.-L. Hao, Z.-X. Yu, W.-X. Wei, L.-D. Lu, X. Wang, Mol. Phys. 2009, 107, 223–235.
- [70] R. P. Samy, S. Ignacimuthu, J. Ethnopharmacol. 2000, 69, 63–71.
- [71] Y. Park, S.-C. Park, H.-K. Park, S. Y. Shin, Y. Kim, K.-S. Hahm, Biopolymers 2007, 88, 199–207.
- [72] C.-F. Chi, B. Wang, Y.-M. Wang, B. Zhang, S.-G. Deng, J. Funct. Foods 2015, 12, 1–10.
- [73] K. Shimada, K. Fujikawa, K. Yahara, T. Nakamura, J. Agric. Food Chem. 1992, 40, 945–948.

Manuscript received: July 24, 2023